Article

Controlling the Antimicrobial Action of Surface Modified Magnesium Hydroxide Nanoparticles

Ahmed F. Halbus [1,2], Tommy S. Horozov [1] and Vesselin N. Paunov [1,*]

[1] Department of Chemistry and Biochemistry, University of Hull, Hull HU67RX, UK;
    a.f.al-mamoori@2014.hull.ac.uk (A.F.H.); t.s.horozov@hull.ac.uk (T.S.H.)
[2] Department of Chemistry, College of Science, University of Babylon, Hilla, Iraq
*   Correspondence: V.N.Paunov@hull.ac.uk; Tel.:+44-1482-465660

Abstract: Magnesium hydroxide nanoparticles ($Mg(OH)_2NPs$) have recently attracted significant attention due to their wide applications as environmentally friendly antimicrobial nanomaterials, with potentially low toxicity and low fabrication cost. Here, we describe the synthesis and characterisation of a range of surface modified $Mg(OH)_2NPs$, including particle size distribution, crystallite size, zeta potential, isoelectric point, X-ray diffraction (XRD), dynamic light scattering (DLS), scanning electron microscopy (SEM), thermogravimetric analysis (TGA), energy dispersive X-ray analysis (EDX), Fourier transform infrared spectroscopy (FTIR), and transmission electron microscopy (TEM). We explored the antimicrobial activity of the modified $Mg(OH)_2NPs$ on the microalgae (*C. reinhardtii*), yeast (*S. cerevisiae*) and *Escherichia coli* (*E. coli*). The viability of these cells was evaluated for various concentrations and exposure times with $Mg(OH)_2NPs$. It was discovered that the antimicrobial activity of the uncoated $Mg(OH)_2NPs$ on the viability of *C. reinhardtii* occurred at considerably lower particle concentrations than for *S. cerevisiae* and *E. coli*. Our results indicate that the antimicrobial activity of polyelectrolyte-coated $Mg(OH)_2NPs$ alternates with their surface charge. The anionic nanoparticles ($Mg(OH)_2NPs/PSS$) have much lower antibacterial activity than the cationic ones ($Mg(OH)_2NPs/PSS/PAH$ and uncoated $Mg(OH)_2NPs$). These findings could be explained by the lower adhesion of the $Mg(OH)_2NPs/PSS$ to the cell wall, because of electrostatic repulsion and the enhanced particle-cell adhesion due to electrostatic attraction in the case of cationic $Mg(OH)_2NPs$. The results can be potentially applied to control the cytotoxicity and the antimicrobial activity of other inorganic nanoparticles.

Keywords: $Mg(OH)_2NPs$; magnesium hydroxide; polyelectrolytes; poly (styrene sulfonate); poly (allyl amine) hydrochloride; antimicrobial nanoparticles; algae; yeast; bacteria; *C. reinhardtii*; *S.cerevisiae*; *E. coli*

1. Introduction

The increased proliferation of infectious illnesses that are caused by microorganisms found in food packaging, medical devices, water treatment systems, and domestic appliances has elicited increased interest [1–3]. The increased resistance of microorganisms against current biocides has caused great concern, particularly for individuals of compromised immune systems [4,5]. This has prompted expanded efforts to investigate new types of nanomaterials as antibacterial agents [6–8], which do not rely on the existing pathways of antimicrobial resistance. Recent studies have been concentrated on antibacterial inorganic nanoparticles, for example, metal oxide nanoparticles, like ZnO, MgO, CuO, Cu_2O, Al_2O_3, TiO_2, CeO_2, and Y_2O_3; metals, e.g., copper, silver, gold etc., metal hydroxides, such as $Mg(OH)_2$ as well as colloids made from biodegradable materials, such as chitosan, lignin, and dextran, loaded with antibacterial agents [9]. $Mg(OH)_2NPs$ have been successfully deployed as

antifungal and antibacterial agents towards different microorganisms [10–12] and there are indications that they can be highly effective [13]. $Mg(OH)_2NPs$ have attracted significant attention over the years due to their wide applications in different fields as an environmentally friendly material with low cost of production [14–17] and they may be potentially used in pharmaceutical formulations [18–21]. However, a limited number of studies have investigated the antimicrobial effects of $Mg(OH)_2NPs$ and reported that the in vivo toxicity values are low, thus demonstrating that it has a non-toxic effect on humans in sensible amounts [22]. Recently, it has been reported that $Mg(OH)_2NPs$ were effective as antibacterial agents towards several bacteria, including *E. coli*, *S. aureus*, *P. aeruginosa,* and *B. phytofirmans* [23–28], and a number of studies have been focused on this new and effective antimicrobial agent [17]. Dong et al. have investigated the antibacterial action of $Mg(OH)_2NPs$ on *Burkholderia phytofirmans* and *Escherichia coli* [24]. Their results indicated that the $Mg(OH)_2NPs$ suspensions are effective towards *B. phytofirmans* and *E. coli.* Their study has also examined the role of the OH^- and Mg^{2+} ions, which are naturally present in the $Mg(OH)_2NPs$ suspension, on the antimicrobial action. They showed that an alkaline medium of pH 10.4, as well as an equivalent amount of Mg^{2+} ions in the aqueous solution. could not kill the bacteria [24]. They have also indicated that $Mg(OH)_2NPs$ can kill *E. coli,* even in dark conditions, which suggested that no photocatalytic properties are involved in their antibacterial action [23]. Hence, the antibacterial mechanism of $Mg(OH)_2NPs$ seems to be very different to those of other metal and metal-based compounds [28–31]. Pan et al. synthesised $Mg(OH)_2NPs$ from three different precursors ($MgCl_2$, $MgSO_4$, and MgO) and tested their antibacterial efficiency towards *E. coli* as a model Gram-negative bacteria [17]. Bactericidal examinations indicated that the antibacterial activity of $Mg(OH)_2NPs$ was inversely related to particle size. Their results also revealed that the ability of $Mg(OH)_2NPs$ to adhere on the bacterial cell walls decreased in the order: $Mg(OH)_{2\_MgCl2} >$ $Mg(OH)_{2\_MgSO4} > Mg(OH)_{2\_MgO}$, which showed that the toxicity of the produced $Mg(OH)_2NPs$ may be caused by the electrostatic interaction induced by secondary adsorption of counter-ions. This means that the type of precursor magnesium salt that is used to produce the $Mg(OH)_2NPs$ by hydrolysis can greatly influence their antimicrobial properties by the secondary absorption of counter-ions on the particles surface. These authors propose that $Mg(OH)_2NPs$ adsorb on the negatively charged bacterial cell wall and somehow disrupt its integrity, and increase its permeability, which kills the bacteria [17].

In this article, we investigate the role of the polymer coating in the antimicrobial activity of $Mg(OH)_2$ nanoparticles that were synthesised by the direct precipitation method. Three different types of microorganisms, *C. reinhardtii*, *S.cerevisiae* cells, and Gram-negative *E. coli* were used to examine the antimicrobial activity of the surface modified $Mg(OH)_2NPs$. In this study, we are interested in using the surface functionalized $Mg(OH)_2NPs$ as innovative anti-algal, anti-bacterial, and antifungal agents. As *C. reinhardtii* is a typical representative of the algae genre and *S. cerevisiae* is a fungal microorganism, they are a good proxy for these assessments. We explored the relationship between the antifungal and antibacterial effect of the particle size, surface charge, in addition to their adhesion to the microbial cell wall. The size of the $Mg(OH)_2NPs$ is likewise essential for their potential activity, as smaller particles have higher portability to relocate between the biological compartments [32]. Moreover, the surface charge of the $Mg(OH)_2NPs$ determines their ability to electrostatically interact with the biological membranes. The present study investigates the impact of the $Mg(OH)_2NPs$ concentration, their zeta potential, and particle size on the viability of *C. reinhardtii, S.cerevisiae,* and *E. coli* at different exposure times. We explore the antimicrobial activity and the nanoparticle internalisation between *C. reinhardtii, S.cerevisiae,* and *E. coli*. In our experiments with surface functionalized $Mg(OH)_2NPs$ on microbial cells, which were systematically done on *C. reinhardtii, S.cerevisiae,* and *E. coli*, we have tested their effect in the absence of growth media whose components may potentially interfere with the particle surface charge. This would lead to ambiguity in the results, depending of the media composition and concentration. To avoid this, we remove the microbial cells from the media prior to testing the effect of the surface functionalized $Mg(OH)_2NPs$ on them. We investigate the antibacterial activity of $Mg(OH)_2NPs$ that are coated with anionic and cationic polyelectrolytes. Our working hypothesis is that coating the $Mg(OH)_2NPs$ with cationic polyelectrolytes may enhance their antimicrobial activity,

while coating them with anionic polyelectrolytes as an outer layer may lead to decreased antibacterial activity because of their electrostatic repulsion from the bacterial cell wall (Figure 1).
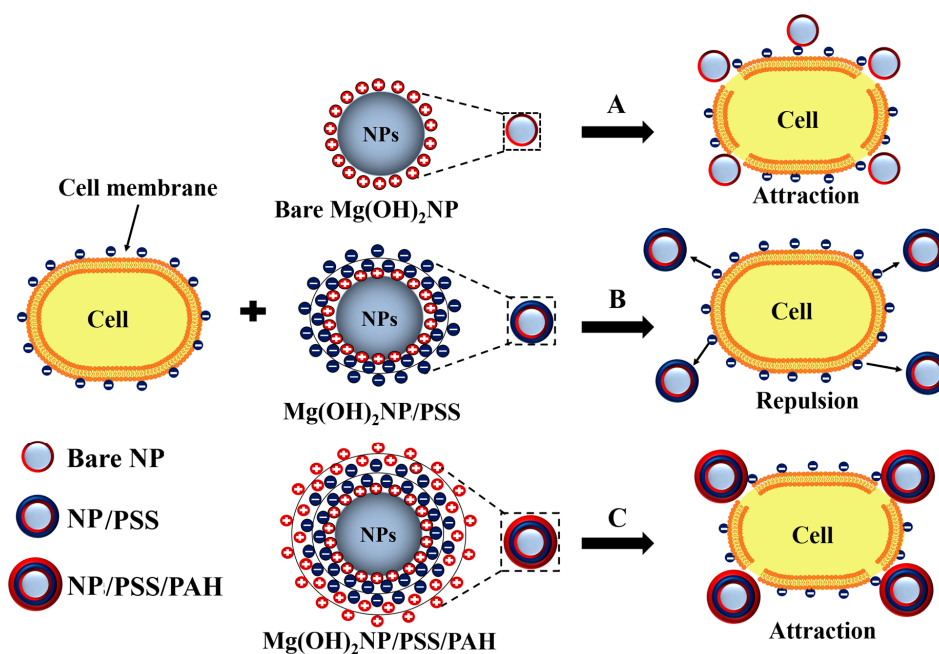
Figure 1. Schematic diagram showing the various contacting patterns between the bare and polyelectrolyte-coated Mg(OH)$_2$NPs on cells. (**A** and **C**) The adhesion of the uncoated and cationic polyelectrolyte-coated Mg(OH)$_2$NPs to the cell wall surfaces is favoured due to their opposite surface charges. (**B**) The interaction between the anionic outer surface of the cell membrane and the Mg(OH)$_2$NPs coated with anionic polyelectrolyte is repulsive. The cationic Mg(OH)$_2$NPs and Mg(OH)$_2$NPs/PSS/PAH nanoparticles are expected to be more effective against the microbial cells than the anionic Mg(OH)$_2$NPs/PSS particles.

2. Materials and Methods

2.1. Materials

Magnesium chloride (98%, Sigma Aldrich, UK), sodium hydroxide (99.6%, Fisher, UK), and fluorescein diacetate (FDA, 98%, Fluka, UK) were used as supplied. Poly(sodium 4-styrene sulfonate) sodium salt (PSS), average M.W. 70 kDa, and poly(allylamine hydrochloride) (PAH), average M.W. 15 kDa, were purchased from Sigma Aldrich, UK. Deionized water that was produced by a Milli-Q reverse osmosis system (Millipore, UK) was used in all of the experiments. *S.cerevisiae* (from Sigma-Aldrich, UK) was cultured, as follows. 10 mg of lyophilised *S.cerevisiae* (baker's yeast) was hydrated in 10 mL of pre-autoclaved deionized water at room temperature. Afterwards, 1 mL of the hydrated yeast suspension was added to 100 mL of the pre-autoclaved YPD culture media (yeast extract, peptone, and dextrose) and incubated for 48 h at 30 °C [33]. *Escherichia coli*, which was sourced from Thermofisher (Invitrogen MAX Efficiency™ DH10B™), was kindly provided for our antibacterial tests by Prof. Rotchell's group at the University of Hull, UK. *E. coli* was grown up using Luria-Bertani medium (LB medium) [34], which can be prepared from 1 g tryptone, 0.5 g yeast extract, and 1 g sodium chloride in 100 mL deionized water. Subsequently, these components were autoclaved for one hour at 1.5 bar at 125 °C. A few microlitres of the stock suspension of *E. coli* were dispersed in the autoclaved culture media next to the Bunsen burner once the culture media was cooled down to room temperature. The cultured *E. coli* was incubated with shaking at 25 °C for 48 h to yield 5×10^5–1×10^6 colony forming units per mL (CFU/mL). Flickinger's group from North Carolina Univeristy, USA kindly provided *Chlamydomonas reinhardtii* (cc-124 strain). This microalgae culture was grown in Tris-Acetate-Phosphate (TAP) culture medium and incubated at a temperature of 30 °C.

The *C. reinhardtii* culture media consisted of TAP salts (NH_4Cl; $MgSO_4 \cdot 7H_2O$; and, $CaCl_2 \cdot 2H_2O$), phosphate buffer solution (PBS), and Hutner's trace elements solution (EDTA disodium salt, $ZnSO_4 \cdot 7H_2O$, H_3BO_3, $MnCl_2 \cdot 4H_2O$, $CoCl_2 \cdot 6H_2O$, $CuSO_4 \cdot 5H_2O$, $FeSO_4 \cdot 7H_2O$, $(NH_4)_6Mo_7O_{24} \cdot 4H_2O$), all purchased from Sigma-Aldrich, UK. The microalgae batch was grown in TAP media at pH 7 while being illuminated for 72 h by a white luminescent lamp with a light intensity of 60 W m^{-2} under constant stirring on a magnetic stirrer.

2.2. Characterisation

The $Mg(OH)_2NPs$ size distribution and the zeta potential were characterised by a Zetasizer Nano ZL instrument (Malvern, UK). A digital sonicator (Branson LTD) was utilized for dispersing the $Mg(OH)_2NPs$ samples at 40% amplitude for 15 min at 2.0 s ON/2.0 s OFF pulse time. The thermogravimetric analysis (TGA) of $Mg(OH)_2NPs$ was done using a Mettler Toledo TGA/DSC instrument under N_2 atmosphere. The crystallite size of $Mg(OH)_2NPs$ at various temperatures was studied by X-ray diffraction (Siemens D5000 X-Ray Diffractometer at 0.15418 nm wavelength). A JEM 2011 (JEOL, Japan) Transmission Electron Microscopy (TEM) machine was used to characterise the particle size and the morphology of $Mg(OH)_2NPs$ on the microbial cells surface. The JEOL JSM-6480 LV SEM instrument was utilized for characterising the morphology of $Mg(OH)_2NPs$ with bacterial.

2.3. Synthesis of $Mg(OH)_2NPs$

The $Mg(OH)_2NPs$ were prepared from magnesium chloride ($MgCl_2$) as a source of magnesium ions and sodium hydroxide (NaOH) aqueous solutions. Precipitation was induced by a dropwise addition of 0.4 M NaOH into the 0.2 M $MgCl_2$ solution under continuous stirring at different reaction temperatures (i.e., 25 °C, 50 °C, 75 °C and 100 °C) for 1 h. The white product was centrifuged and washed with copious amounts of high purity water and ethanol for the effective removal of impurities. The final product was dried at 80 °C for 24 h [6]. Aqueous dispersions of the $Mg(OH)_2NPs$ were then prepared by dispersing 0.025 g of the $Mg(OH)_2$ sample in 100 mL deionized water by using a digital sonicator (Branson Ltd.) at 40% of the maximum power for 15 min at 2 s ON/2 s OFF pulse time. Figure S1 shows a schematic diagram of the synthesis method of $Mg (OH)_2NPs$.

2.4. Preparation of Polyelectrolyte-Coated $Mg(OH)_2NPs$

Polyelectrolyte-coated $Mg(OH)_2NPs$ were prepared by using the $Mg(OH)_2NPs$ synthesised at a reaction temperature of 75 °C. 50 mL of 1000 µg mL^{-1} $Mg(OH)_2NPs$ dispersion in deionized water were added dropwise to an equal amount of 50 mg mL^{-1} PSS (M.W. ~70 kDa) solution in 1 mM NaCl. The samples were washed three times by centrifugation for 1 h at 10,000 rpm to remove the excess of PSS after shaking for 1 h on orbital shaker. Finally, the PSS-coated $Mg(OH)_2NPs$ were re-dispersed in 50 mL deionized water [35] and the particle size and zeta potential measured by a Zetasizer Nano ZL instrument. To prepare the PAH-coated nanoparticles, the PSS-coated $Mg(OH)_2NP$ suspension was mixed dropwise with 50 mL of 50 mg mL^{-1} PAH (M.W. 15 kDa) that was dissolved in 1 mM NaCl solution. The mixture was shaken for 20 min and centrifuged three times at 10,000 rpm for one hour to yield $Mg(OH)_2NPs/PSS/PAH$.

2.5. Antimicrobial Assay of Polyelectrolyte-Coated $Mg(OH)_2NPs$ on S.cerevisiae

The effect of $Mg(OH)_2NPs$ on *S.cerevisiae* cells was examined after removing the cells from the culture media. 30 mL dispersion of *S.cerevisiae* cells were washed by centrifugation with deionized water three times, and then re-dispersed in 30 mL deionized water. 5 mL of *S.cerevisiae* cell dispersion in deionized water were incubated with 5 mL $Mg(OH)_2NPs$ aqueous suspension upon increasing total particle concentrations (0, 250, 500, 1000, 2500, and 5000 µg mL^{-1}) for 10 min, 6 h, 12 h, and 24 h. 1 mL of each incubated *S.cerevisiae* sample was centrifuged at 3500 rpm for 4 min and washed with deionized water to remove the excess of $Mg(OH)_2NPs$. The *S.cerevisiae* cells were re-suspended in 1 mL of deionized water, then two drops of 1 mM FDA solution in acetone were added to each sample and

then mixed together for 15 min. After that, the samples were washed three times with deionized water by centrifugation at 3500 rpm for 4 min. Finally, the viability of the cells was examined by fluorescence microscopy and an automatic cell counter (Nexcelom Cellometer Auto X4 Fluorescence). Similar experiments were utilized to test the effect of $Mg(OH)_2$NPs that were coated with polyelectrolytes on the viability of *S.cerevisiae*.

2.6. Antibacterial Assay of Polyelectrolyte-Coated Mg(OH)₂NPs on E. coli

10 mL of the *E. coli* culture grown in LB medium was washed, centrifuged three times with deionized water at 5000 rpm for three minutes, and redispersed in 100 mL deionized water. Subsequently, 5 mL of the washed *E. coli* suspension were incubated with a series of 5 mL aliquots of aqueous dispersions of $Mg(OH)_2$NPs of different concentrations (0, 250, 500, 750, 1000, 2500, 5000, and 6000 $\mu g\ mL^{-1}$). After each incubation, 1 mL of each *E. coli* suspension sample was washed and re-suspended in 1 mL deionized water. Afterwards, 100 μL of culture media free *E. coli* bacteria were incubated with 100 μL of the BacTiter-Glo Microbial cell viability reagent in a white opaque 96-well solid flat bottom microplate, shaken for 30 s, and then incubated for five minutes at 25 °C. The relative luminance was measured as a function of incubation time to find out the cell viability upon incubation with different concentration of $Mg(OH)_2$NPs. The same experiments were also repeated with polyelectrolyte-coated $Mg(OH)_2$NPs. This was done by incubating an aliquot of the *E. coli* suspension (diluted 10 times) with $Mg(OH)_2$NPs that were coated with poly(sodium-4-styrenesolfonate and poly(allylamine hydrochloride) for up to 24 h.

2.7. Antialgal Activity of Polyelectrolyte-Coated Mg(OH)₂NPs to C. reinhardtii

50 mL of *C. reinhardtii* culture were washed from the culture media three times by using deionized water and centrifugation, and finally re-dispersed in 30 mL deionized water. 5 mL of the washed *C. reinhardtii* cells were incubated with a series of 5 mL aliquots of aqueous $Mg(OH)_2$NPs dispersions at different concentrations at 25 °C. A control sample of the same cells was treated in a similar way without any exposure to $Mg(OH)_2$NPs. After that, 1 mL of the *C. reinhardtii* suspension was taken from each treated sample and washed with deionized water to remove the excess of nanoparticles by centrifugation at 3500 rpm for 4 min. The *C. reinhardtii* cells were re-suspended in 1 mL deionized water, and two drops of 1 mM FDA solution in acetone were added to each sample and mixed together for 15 min. After that, the samples were washed three times with deionized water by centrifugation at 3500 rpm for 4 min. Finally, the automatic cell counter was utilized to assay the microalgae cell viability. The same method was used to test the effect of $Mg(OH)_2$NPs that were coated with PSS and PAH on the viability of *C. reinhardtii*, which were incubated at different particle concentrations for various exposure times.

2.8. SEM and TEM Sample Preparation Protocol for C. reinhardtii, S.cerevisiae and E. coli after Exposure to Bare- and Polyelectrolyte-Coated Mg(OH)₂NPs

The *C. reinhardtii*, *S.cerevisiae* and *E. coli* were washed by centrifugation and then fixed with 2.5% glutaraldehyde at room temperature for two hours in 0.1M cacodylate buffer pH 7.2 after incubation with the bare- or polyelectrolyte-coated $Mg(OH)_2$NPs of various concentrations. These samples were then post-fixed in 1% osmium tetroxide for 1 h, and then dehydrated in a range of ethanol-water mixtures with an increasing ethanol content from 50 vol% up to 100 vol%, followed by a critical point drying. After incubation with $Mg(OH)_2$NPs, the microbial cells were prepared for TEM imaging while using the following procedure. The cells were washed with deionized water to remove the excess of $Mg(OH)_2$NPs by centrifugation at 500 rpm and then fixed in 2 wt% glutaraldehyde for one hour at room temperature. This was followed by a treatment with 1 wt% osmium tetroxide for one hour. Subsequently, the samples were incubated for one hour with 2.5% uranyl acetate and washed with aqueous ethanol solutions of increasing concentration, as described above. After standard dehydration, the microbial samples were embedded in fresh epoxy/Araldite at 60 °C for two days, left for two

days at room temperature, and sectioned with an ultra-microtome. SEM and TEM imaged microbial samples before and after the nanoparticle treatment.

2.9. Zeta Potential Measurements of the C. reinhardtii, S.cerevisiae and E. coli cells after treatment with Mg(OH)$_2$NPs

The changes of surface charge of *C. reinhardtii, S.cerevisiae,* and *E. coli* after exposure to Mg(OH)$_2$NPs at different concentrations (0, 250, 500, 750, 1000, 2500, 5000, and 6000 μg mL^{-1}) were determined by a Zetasizer Nano ZL instrument (Malvern, UK). The cells were removed from the excess of Mg(OH)$_2$NPs in the aqueous phase by centrifugation, and then dispersed in deionized water. For each sample, an appropriate amount of undiluted solution was placed into the cuvette, and an average zeta potential value was obtained from three individual measurements. The solution media was deionized water in all of the zeta potential measurements.

2.10. MIC of Non-modified and PSS/PAH-coated Mg(OH)$_2$NPs on Microbial Cells

The following protocol was used to determine the Minimal Inhibitory Concentration (MIC) of Mg(OH)$_2$NPs and PSS/PAH-coated Mg(OH)$_2$NPs on cells. A negative control of 100 μL of LB medium was added to the first line of wells of a 96 well plate. 50 μL of LB medium were added to the treatment wells and the positive bacteria control wells. A stock solution of Mg(OH)$_2$NPs and PSS/PAH-coated Mg(OH)$_2$NPs was created in fresh LB medium to a total volume of 10 mL. 50 μL of this formulation ware added to the first line of treatment wells, and serial diluted 1:2 across the 96 well plate, which ensured that it was mixed by pipetting up and down within each well. An overnight culture of *E. coli* was diluted into a sterilised 0.85% saline until an absorbance reading between 0.08 and 0.12 at 625 nm was obtained on a spectrophotometer (0.5 Mcfarland Standard). The saline diluted bacteria were further diluted 1:150 into LB (10 mL LB + 66.67 μL of bacteria in saline solution) yielding a 10 mL stock containing 5×10^5–1×10^6 cells per mL. 50 μL from this bacteria stock were added to each treatment and positive bacteria control wells, seeding with 2.5×10^4–5×10^4 cells per well. Each well contained a final volume of 100 μL, with decreasing concentrations of treatment on equal amounts of bacteria. The plate was incubated for 24 h at 37 °C. After incubation, 20 μL of resazurin solution were added to each well. The MIC was determined from the lowest concentration treatment, which inhibited growth.

3. Results and Discussion

3.1. Preparation and Characterisation of Mg(OH)$_2$NPs

The mean hydrodynamic diameter and zeta potential of the Mg(OH)$_2$NPs in deionized water were measured by the dynamic light scattering instrument (DLS) of suspensions that were prepared by dispersing 0.025 g of Mg(OH)$_2$NPs sample in 100 mL of deionized water by a digital sonicator. The average hydrodynamic diameter of Mg(OH)$_2$NPs was found to be 69 ± 10 nm and their zeta potential was +30 ± 6 mV, as shown in Figure S2 and Figure S3. The thermo gravimetric analysis (TGA) that was carried out between 50 and 1000 °C, as shown in Figure S4A, indicated that the Mg(OH)$_2$ sample was stable up to 270 °C. Subsequently, the endothermic peak corresponding to the removal of the adsorbed water molecules took place between 270–300 °C, as also reported by other authors [36]. The major weight loss step has been found in the temperature range of 300–450 °C, which is due to the transition phase, corresponding to the decomposition of Mg(OH)$_2$NPs to MgO. The TGA curve exhibits a total mass loss equal to 29.46%, which is slightly lower than the calculated mass loss (30.8%) that is attributed to the complete dehydroxylation process of Mg(OH)$_2$. This result also agrees with previous studies [36–38]. An Energy dispersive X-ray Diffraction (EDX) analysis was carried out on the synthesised Mg(OH)$_2$NPs to verify the elemental composition. The EDX data in Figure S4B confirm the presence of magnesium and oxygen signals in the Mg(OH)$_2$NPs sample. The elemental analysis of the Mg(OH)$_2$NPs yielded 36.59% of magnesium and 59.94% of oxygen, which indicates that the formed Mg(OH)$_2$NPs were in its highly purified form and in agreement with previous studies [24].

We studied the effect of annealing temperature on the particle size of $Mg(OH)_2NPs$ for the synthesis that was done at various reaction temperature (25 °C, 50 °C, 75 °C, and 100 °C). Figure S4C shows the impact of the temperature of the reaction mixture on the size of $Mg(OH)_2NPs$ for one hour. $Mg(OH)_2NPs$ of lower average size were produced at 75 °C and 100 °C, while larger particles were created at 25 °C and 50 °C. Therefore, 75 °C and 100 °C were the optimal temperatures for the production of $Mg(OH)_2NPs$.

The zeta potential and particle size of the produced $Mg(OH)_2NPs$ was measured at pH in the range 3–12 and the results are shown in Figure S4D. The isoelectric point of the non-coated $Mg(OH)_2NPs$ was approximately at pH 11.7, i.e., the bare $Mg(OH)_2NPs$ are cationic at neutral pH. As it can be seen from Figure S4D, the zeta potential decreases and the particle size increases upon the increase of pH. The aggregation of $Mg(OH)_2NPs$ occurs above pH 8.5. The Fourier transform infrared spectroscopy (FTIR) spectrum of the $Mg(OH)_2NPs$ synthesised using a magnesium chloride solution at different reaction temperatures is shown in Figure S5 (ESI). The sharp and intense 3700 cm^{-1} FTIR peak corresponds to the $Mg(OH)_2$ asymmetric O–H stretching. The band at 1400 cm^{-1} is due to the water O–H stretch. The strong and wide 570 cm^{-1} peak is due to Mg−O stretching. No other absorption peaks from impurities were detected. This result indicates that the $Mg(OH)_2$ that was obtained had higher purity and it is also in agreement with previous studies [39,40].

3.2. Effect of the Precipitation Temperature on the Crystallite Size of the Synthesised $Mg(OH)_2NPs$

Figure 2 shows the XRD pattern of $Mg(OH)_2NPs$ samples that were obtained at various reaction temperatures 25 °C, 50 °C, 75 °C, and 100 °C while using magnesium chloride as a precursor. The diffraction peaks are in agreement with the hexagonal structure of $Mg(OH)_2NPs$ according to Joint Committee on Powder Diffraction Standards (JCPDS) Card No. 00-044-1482, which indicates that no apparent impurities are detected. The average crystallite size of $Mg(OH)_2NPs$ was calculated by using the Scherrer equation, $D = K\lambda/\beta\cos\theta$, were D is the crystallite size in nm, K is a dimensionless shape constant taken as 0.94, 2θ is the diffraction angle, λ is the wavelength of the X-ray radiation (CuKα = 0.15406 nm), and β is the full width at the half-maximum (FWHM) of the diffraction peak.
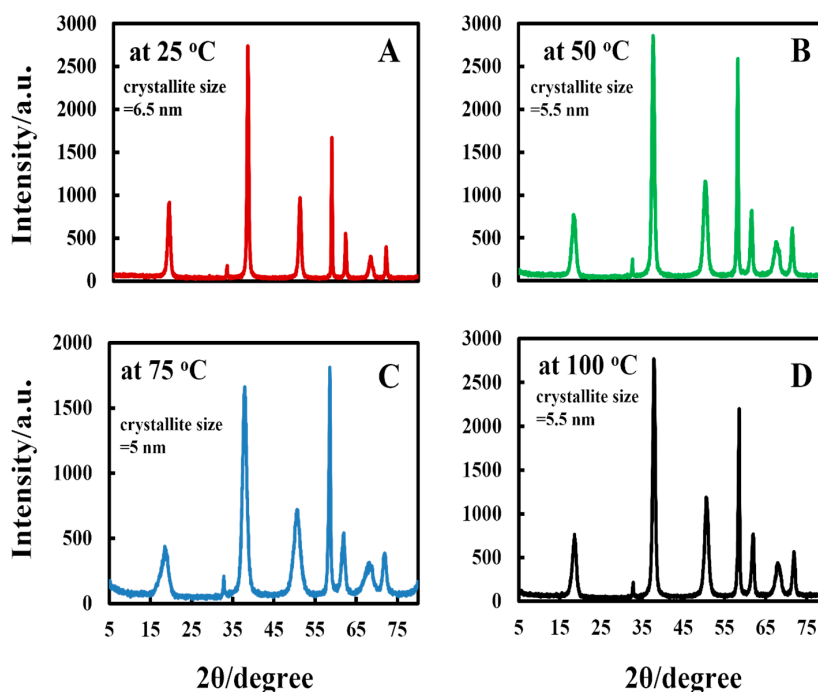
Figure 2. Comparison of the X-ray pattern of $Mg(OH)_2NPs$ precipitated at 25 °C (**A**), 50 °C (**B**), 75 °C (**C**), and 100 °C (**D**).

3.3. Polyelectrolyte-Functionalized Mg(OH)$_2$NPs

We coated 69 nm Mg(OH)$_2$NPs with two subsequent layers of PSS and PAH via the procedures explained above [35]. Figure 3A shows the zeta potential of the coated Mg(OH)$_2$NPs as a function of the number of polyelectrolyte layers. The zeta potential of the Mg(OH)$_2$NPs changed from approximately +30 mV to −36 mV for Mg(OH)$_2$NPs/PSS. Further coating with PAH yielded positively charged Mg(OH)$_2$NPs/PSS/PAH with a zeta potential of +51 mV. As expected, the particle surface charge alternates with the addition of the oppositely charged polyelectrolyte layer. Figure 3B shows that the coated NPs size increases after every subsequent polyelectrolyte coating due to partial aggregation.
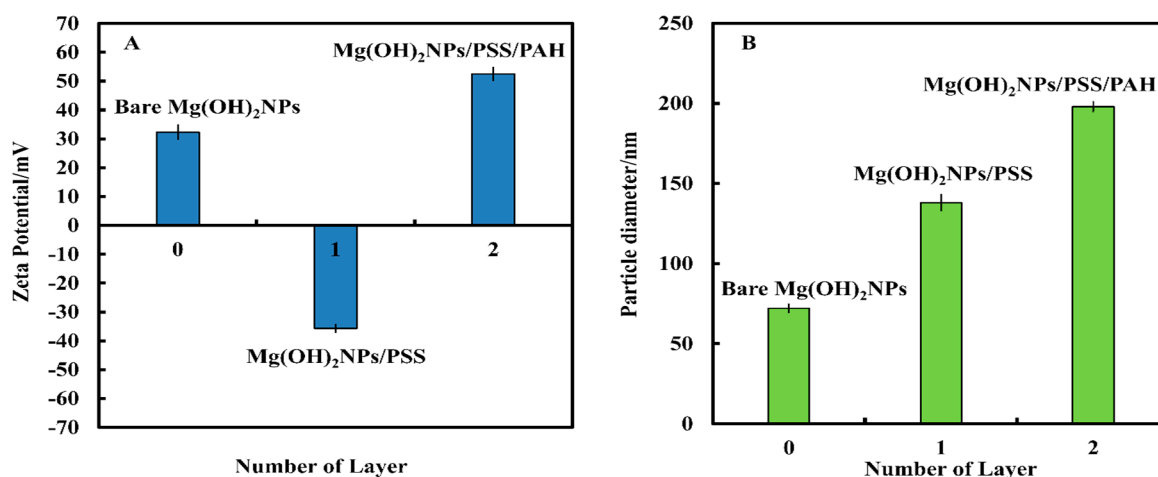
Figure 3. (**A**) The zeta potential and (**B**) particle size of bare-and polyelectrolyte-coated Mg(OH)$_2$NPs.

3.4. Antimicrobial Assay of Bare Mg(OH)$_2$NPs on S.cerevisiae, C. reinhardtii and E. coli

We compared the antimicrobial activity of bare Mg(OH)$_2$NPs on *C. reinhardtii*, *S. cerevisiae*, and *E. coli*, and Figure 4 shows the cell viability. We incubated samples of *S.cerevisiae* cells with dispersed Mg(OH)$_2$NPs at different particle concentrations (0, 250, 500, 1000, 2500, and 5000 µg mL^{-1}) for different periods of time, up to one day. Subsequently, an aliquot of every sample was taken to examine the number of viable *S.cerevisiae* cells while using an automatic cell counter by FDA cell viability assay. Figure 4A shows the percentage of viable *S.cerevisiae* cells at various incubation times (10 min., 6 h, 12 h, and 24 h). One can see that the percentage of viable *S.cerevisiae* after 10 min incubation is at the same level as in the untreated sample. After 6 h of incubation, no measurable antimicrobial effect is noticed up to 500 µg mL^{-1} Mg(OH)$_2$NPs; however, antimicrobial activity is observed at 1000, 2500, and 5000 µg mL^{-1} Mg(OH)$_2$NPs. After 12 h, the viability of *S.cerevisiae* sharply decreases at particle concentrations in the range 500–5000 µg mL^{-1}. After one day of incubation, concentrations higher than 250 µg mL^{-1} bare Mg(OH)$_2$NPs showed measurable antimicrobial activity towards *S.cerevisiae*. The optical microscopy examination of these samples suggests that the *S.cerevisiae* cells aggregate at a high particle concentration. Our results indicate a strong decline of the *S.cerevisiae* cell viability at concentrations above 1000 µg mL^{-1} bare Mg(OH)$_2$NPs. Figure S15 (ESI) shows the same data, as in Figure 4A–C in CFU mL^{-1}.

The data in Figure 4A suggest that, at high concentrations of bare Mg(OH)$_2$NPs, they electrostatically adhere to the negatively charged cell membranes, which subsequently kills the cells. The attachment of Mg(OH)$_2$NPs to the cells was also examined by TEM imaging. Figure 5A,C show TEM images of the *S.cerevisiae* cells before and after treatment with 1000 µg mL^{-1} Mg(OH)$_2$NPs solution for 24 h. Those are compared with the untreated samples of *S.cerevisiae* that are shown in Figure 5A,B. The TEM images show that, before the treatment (Figure 5A), the membrane of the *S.cerevisiae* cells is regular and smooth, the treatment with 1000 µg mL^{-1} Mg(OH)$_2$NPs leads to a significant accumulation of Mg(OH)$_2$NPs on the external wall of *S.cerevisiae* at such a high particle concentration (Figure 5C).
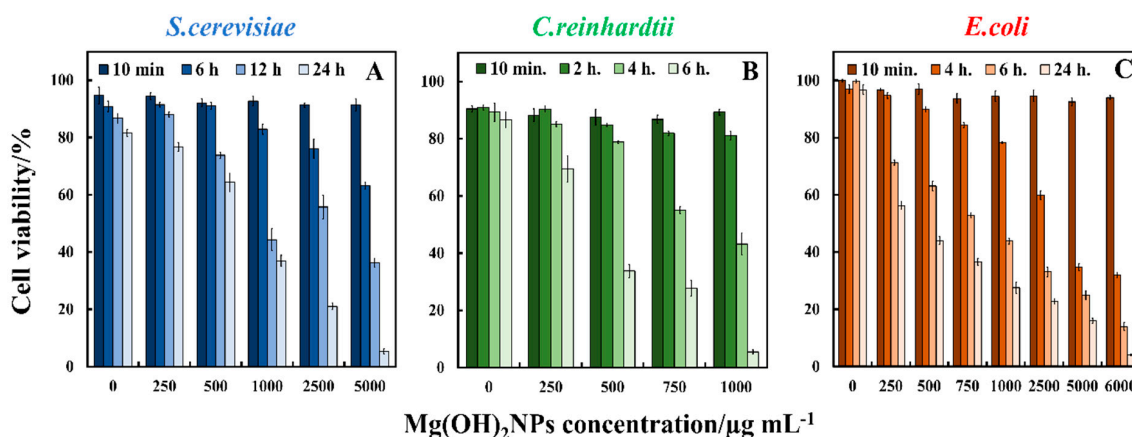
Figure 4. The antimicrobial activity of bare Mg(OH)$_2$NPs on (**A**) *S.cerevisiae* (**B**) *C. reinhardtii* and (**C**) *E. coli* at various particle concentrations. The cells were incubated with the Mg(OH)$_2$NPs at different periods of time shown.
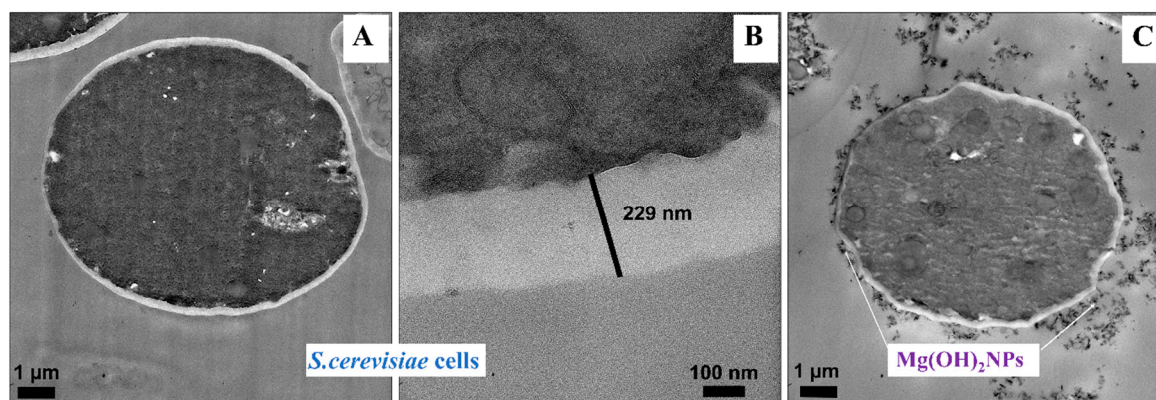
Figure 5. Transmission electron microscopy (TEM) images of *S. cerevisiae* after being incubated for one day with bare Mg(OH)$_2$NPs: (**A**) A control sample without Mg(OH)$_2$NPs. (**B**) A high-resolution TEM image of the *S. cerevisiae* wall without Mg(OH)$_2$NPs. (**C**) *S. cerevisiae* cells incubated with 1000 μg mL^{-1} Mg(OH)$_2$NPs showing the attachment of Mg(OH)$_2$NPs to the outer cell surface.

We also confirmed these results by EDX of the treated *S. cerevisiae* cells, which showed the presence of Mg on the outer part of the cell membrane (Figure S6, ESI). Although the exposure of the *S. cerevisiae* cells to bare Mg(OH)$_2$NPs at concentration 1000 μg mL^{-1} caused a cytotoxicity effect (Figure 5C), it did not cause an internalisation of Mg(OH)$_2$NPs, as the cell wall of *S. cerevisiae* cells is very thick (200 nm, Figure 5B) when compared to other microbial cells. We envisage two probable mechanisms for the antimicrobial effect of Mg(OH)$_2$NPs on yeast. There is a significant accumulation of Mg(OH)$_2$NPs on the cell membranes due to their cationic nature at neutral pH. As these particles have very irregular morphology and they consist of smaller crystallites, their adhesion to the cell membrane in large amounts can potentially cause its dislocation and cracking. Local damage of the membrane may lead to cell viability loss although we do not observe a straight permeation of Mg(OH)$_2$NPs to the *S.cerevisiae* wall. Another possible mechanism of membrane damage can be caused by the counter-ion atmosphere of the Mg(OH)$_2$NPs, which consists of highly concentrated hydroxyl ions (OH$^-$) of very high local pH which can cause lipid hydrolysis on the membrane surface and killing the cell. Some of these mechanisms have been commented on by other authors for uncoated Mg(OH)$_2$NPs [17,24,28].

We also examined the antimicrobial activity of Mg(OH)$_2$NPs towards *C. reinhardtii* under similar conditions for various exposure times, as shown in Figure 4B. At a 10 min exposure time, all of the *C. reinhardtii* were viable at the similar level as the untreated sample. After two hours of incubation, the *C. reinhardtii* viability declined for Mg(OH)$_2$NPs concentrations from 250 μg mL^{-1} to 1000 μg

mL^{-1}. After 4 h, the *C. reinhardtii* viability was reduced to 40% at 1000 µg mL^{-1} of Mg(OH)$_2$NPs, while, after 6 h, it sharply declined for 250 µg mL^{-1} to 1000 µg mL^{-1} concentrations of Mg(OH)$_2$NPs, which led to the complete loss of cell viability at concentrations above 750 µg mL^{-1} Mg(OH)$_2$NPs. Figure 6 shows TEM images of *C. reinhardtii* exposed to Mg(OH)$_2$NPs at various concentrations. TEM images of the *C. reinhardtii* after 6 h of incubation with Mg(OH)$_2$NPs indicate the localization of the Mg(OH)$_2$NPs with respect to the cell membrane. One can see that the outer cell wall of *C. reinhardtii* obtained a thick layer of associated NPs after treatment with 750 µg mL^{-1}, 1000 µg mL^{-1} and 5000 µg mL^{-1} concentrations of Mg(OH)$_2$NPs (Figure 6C–F). The internalization of Mg(OH)$_2$NPs in the *C. reinhardtii* was not observed, even at 5000 µg mL^{-1} Mg(OH)$_2$NPs, as shown in Figures S7 and S8. The EDX shows the absence of Mg in the inside of *C. reinhardtii,* but confirms its presence on the outer wall.
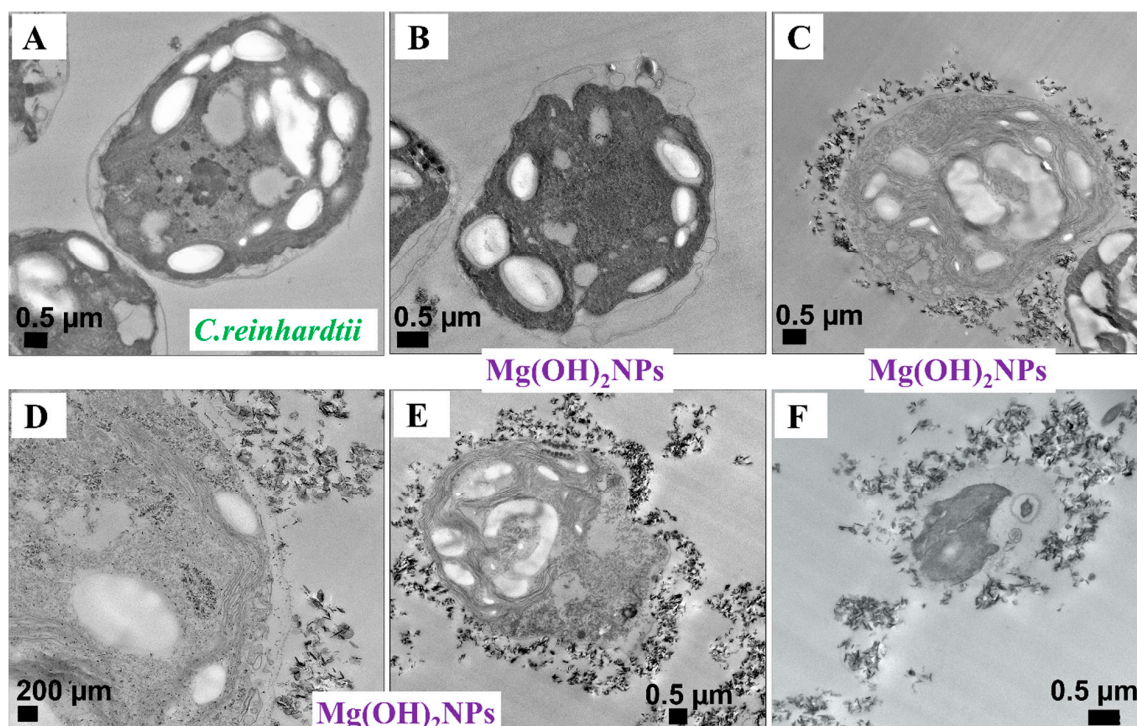
Figure 6. TEM images of *C. reinhardtii* after being exposed to 0, 250, 750, 1000 and 5000 µg mL^{-1} Mg(OH)$_2$NPs for six hours (fixed, embedded in resin and sectioned). (**A**) An untreated sample without Mg(OH)$_2$NPs; (**B**) *C. reinhardtii* treated with 250 µg mL^{-1} Mg(OH)$_2$NPs; (**C**) and (**D**) *C. reinhardtii* incubated with 750 µg mL^{-1} Mg(OH)$_2$NPs at different magnifications. (**E**) and (**F**) *C. reinhardtii* treated with 1000 µg mL^{-1} and 5000 µg mL^{-1} Mg(OH)$_2$NPs, respectively.

Figure 4C shows the results for the effect of bare Mg(OH)$_2$NPs towards *E. coli* at various incubation times. The data demonstrate that the bare Mg(OH)$_2$NPs have excellent antimicrobial effects on the *E. coli* at 6000 µg mL^{-1} for one day. The *E. coli* viability sharply decreases for treatment with 6000 µg mL^{-1} Mg(OH)$_2$NPs after four hours of exposure. The viability decreases further after six hours and, after one day, it resulted in approximately 97% loss of viability. Past research suggested that the antibacterial effect might be credited to multiple factors: (i) the cellular internalization of NPs where they could potentially interfere with the bacterial DNA and cellular organelles [41–45]; (ii) immediate contacts with the bacterial cell wall [23,24]; and, (iii) the increased local dissolution of metal ions of the nanoscale metal oxide [46,47]. Usually, the antimicrobial impact is dependent on the size of the nanoparticles and a better antimicrobial effect is achieved with smaller nanoparticles [17,48–50].

The Mg(OH)$_2$NPs with the smallest size (about 70 nm) had the highest antimicrobial activity. We undertook TEM imaging and EDX analysis to examine the location of magnesium in the *E. coli*

after treating them with non-coated Mg(OH)$_2$NPs. Magnesium was not detected by the EDX in many randomly selected regions inside the *E. coli*, but it was primarily found on the outer side of the cell wall, as shown in Figure S9 (ESI). This showed that the dissolved magnesium ions and Mg(OH)$_2$NPs did not go to the inside of *E. coli*. Nevertheless, evident changes of the *E. coli* cell structure were seen after incubation with Mg(OH)$_2$NPs. Figure 7D shows the images of untreated *E. coli*, where the bacteria have preserved the integrity of their cell walls. After incubation with 2500 µg mL^{-1} (7E) and 5000 µg mL^{-1} (7F) Mg(OH)$_2$NPs for one day, the cell profile became fussy and the walls of *E. coli* appear as disintegrated. Therefore, the antimicrobial activity of Mg(OH)$_2$NPs might be expressed more via their adsorption on the outer side of the cell wall, rather than through internalization in the cell, which leads to the decay of the cell walls of *E. coli*. Furthermore, SEM imaging was used to study the presence of Mg(OH)$_2$NPs on the surfaces of the bacteria. Figure 7A–C show *E. coli* samples after being treated with 2500 µg mL^{-1} and 5000 µg mL^{-1} Mg(OH)$_2$NPs for one day. They indicate that the cell wall has a build-up of a dense layer of nanoparticles. Moreover, EDX indicated that the samples contain magnesium, and confirmed that the Mg(OH)$_2$NPs have the ability to adhere on the bacterial cell wall with occasional penetration on the inside. Consequently, the *E. coli* lack of viability is associated with the compromised integrity of bacteria walls, which is seen by SEM and TEM for these samples. This is consistent with the mechanisms outlined above which indicates that the antimicrobial action of Mg(OH)$_2$NPs on the cells is likely to be due to the cationic character of Mg(OH)$_2$NPs that adsorb on the negatively charged bacterial cell wall by electrostatic attraction. The adsorbed Mg(OH)$_2$NPs disrupt the integrity of the bacterial cell wall, which then increases its permeability and kills the bacteria.
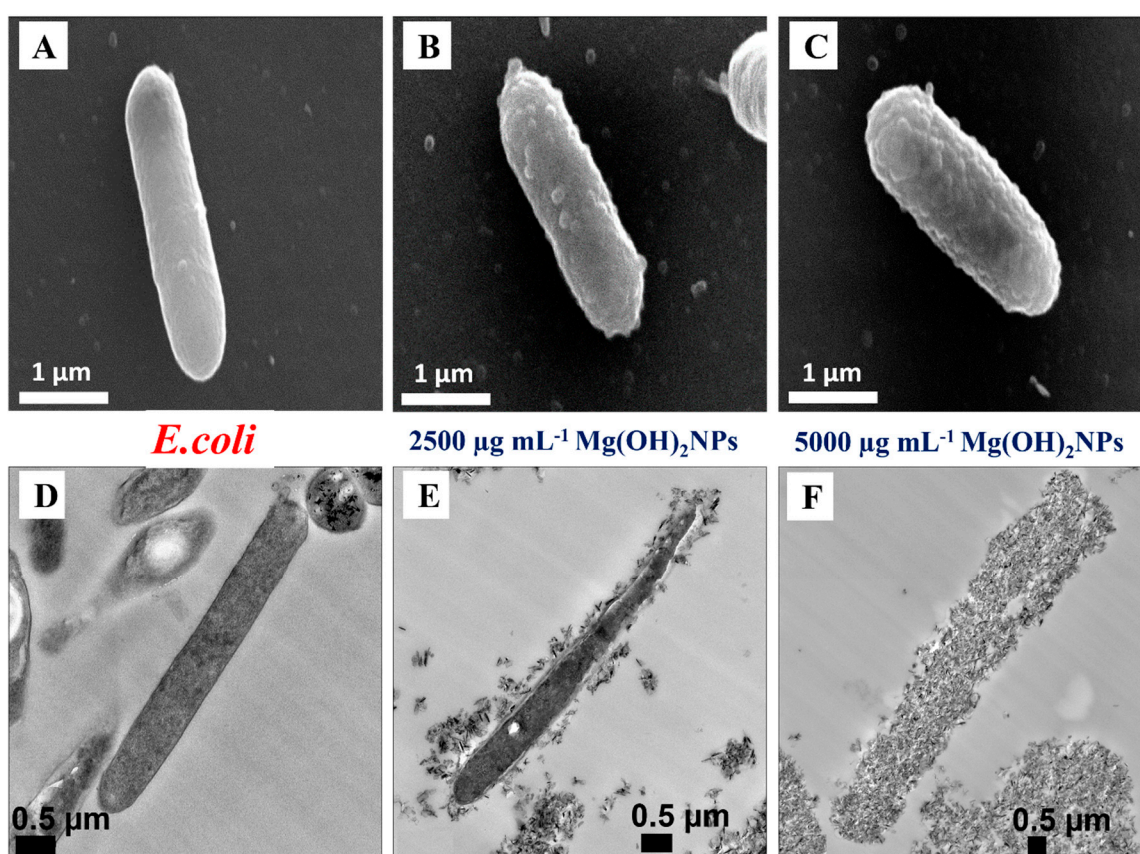
Figure 7. Scanning electron microscopy (SEM) and TEM images of *E. coli* after being incubated for 24 h with a suspension of bare Mg(OH)$_2$NPs: (**A**) SEM and (**D**) TEM images of an untreated sample. (**B**) SEM and (E) TEM images of *E. coli* incubated with 2500 µg mL^{-1} Mg(OH)$_2$NPs. (**C**) SEM and (**F**) TEM images of *E. coli* incubated with 5000 µg mL^{-1} Mg(OH)$_2$NPs.

3.5. Zeta Potential Measurements of Cells after Treatment with Mg(OH)₂NPs

We further explored the effect of the particles attachment on the outer cell wall, as it may play a significant role on their antimicrobial action [17,24,28]. We studied the zeta potential of the *S.cerevisiae*, *C. reinhardtii,* and *E. coli* after treatment with Mg(OH)₂NPs in solution. The cells were incubated with Mg(OH)₂NPs suspensions at different particle concentrations. Subsequently, an aliquot of every suspension was taken to examine the cells average zeta potential value by a Zetasizer instrument. We found that Mg(OH)₂NPs have an average zeta potential of +30 ± 6 mV. Upon incubation with bare Mg(OH)₂NPs, the *S.cerevisiae* cells, which are negatively charged (zeta potential of −12 ± 5 mV), still were shown to be negative, but significantly reduced by magnitude zeta potential due to a build–up of cationic NPs, as shown in Figure 8A. Note that the zeta potential of threated cells does not vary much with the duration of the treatment.
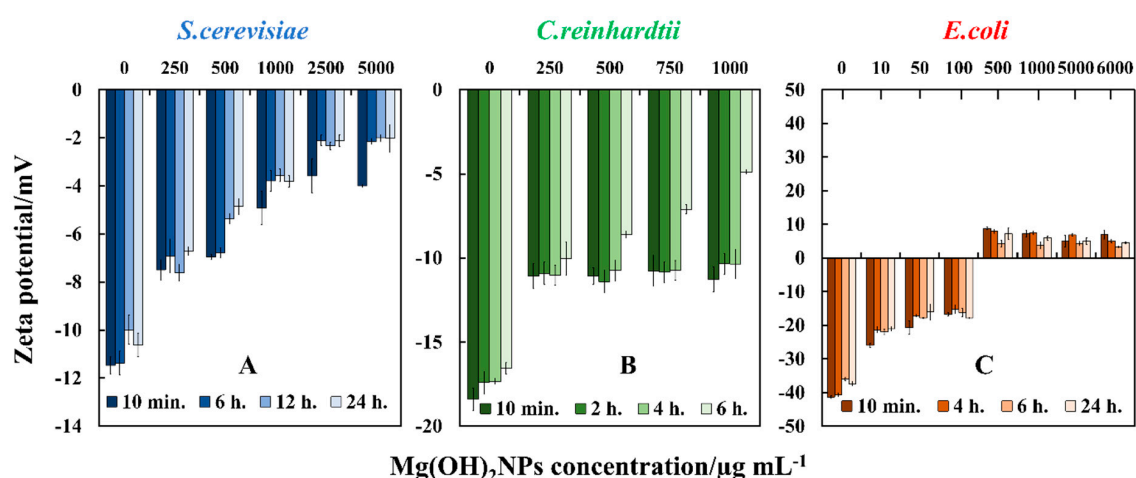
Figure 8. The zeta potential of cells treated with different concentrations of Mg(OH)₂NP suspensions at various incubation times: (**A**) *S.cerevisiae,* (**B**) *C. reinhardtii,* and (**C**) *E. coli* cells.

The *C. reinhardtii* cells that have a negative zeta potential of −18 ± 5mV also reduced their zeta potential by magnitude after treatment with the cationic Mg(OH)₂NPs, but did not charge reverse, even at high particle concentrations, as presented in Figure 8B. Figure 8C shows the impact of bare Mg(OH)₂NPs on the *E. coli* zeta potential. *E. coli* cells, which carried negative charge (zeta potential −41±5 mV), remained negatively charged when treated with up to 100 µg mL⁻¹ Mg(OH)₂NPs. At higher Mg(OH)₂NPs concentration, the zeta potential of *E. coli* cells turned positive when exposed to 500 µg mL⁻¹ to 6000 µg mL⁻¹ Mg(OH)₂NPs. These results show that the adhesion of Mg(OH)₂NPs to cells might indeed be primarily driven by electrostatic interactions [17,51]. It can be concluded that the positive charge of Mg(OH)₂NPs has high impact on the adsorption of particles on the cells membrane. The SEM and TEM images confirmed this (Figure 6).

3.6. Antimicrobial Assay of Polyelectrolyte-Coated Mg(OH)₂NPs on S.cerevisiae, C. reinhardtii, and E. coli

We studied the antimicrobial activity of Mg(OH)₂NPs that were coated with multilayers of polyelectrolytes on *S.cerevisiae, C. reinhardtii,* and *E. coli*. We functionalized Mg(OH)₂NPs with PSS and PAH and compared their antimicrobial effect with that of the bare Mg(OH)₂NPs. The aqueous suspensions of *S.cerevisiae* were incubated with Mg(OH)₂NPs/PSS and Mg(OH)₂NPs/PSS/PAH suspensions at various particle concentrations (0, 250, 500, 1000, 2500, and 5000 µg mL⁻¹) for up to one day. The results represented in Figure 9A show that the anionic Mg(OH)₂NPs/PSS have a lower antimicrobial activity on *S.cerevisiae* when compared to the cationic bare Mg(OH)₂NPs (c.f. Figure 4A). No change in the *S.cerevisiae* viability was registered for Mg(OH)₂NPs/PSS, even at high particle concentrations, at incubating times up to six hours. The same treatment with the cationic Mg(OH)₂NPs/PSS/PAH showed a significant antimicrobial activity on *S.cerevisiae* at particle

concentrations of 1000, 2500, and 5000 μg mL^{-1}, as shown in Figure 9B. A very strong effect of the Mg(OH)$_2$NPs/PSS/PAH on *S.cerevisiae* viability was observed upon their incubation with high particle concentrations of 5000 μg mL^{-1} for up to 24 h. In contrast, upon incubation with the anionic Mg(OH)$_2$NPs/PSS at high particle concentrations of 5000 μg mL^{-1}, we observed a moderate impact on *S.cerevisiae* viability for up to one day of incubation (Figure 9A). Figure S12 compares the anti-yeast activity bare Mg(OH)$_2$NPs with Mg(OH)$_2$NPs/PSS and Mg(OH)$_2$NPs/PSS/PAH as a function of the nanoparticle concentration for 24 h of exposure.
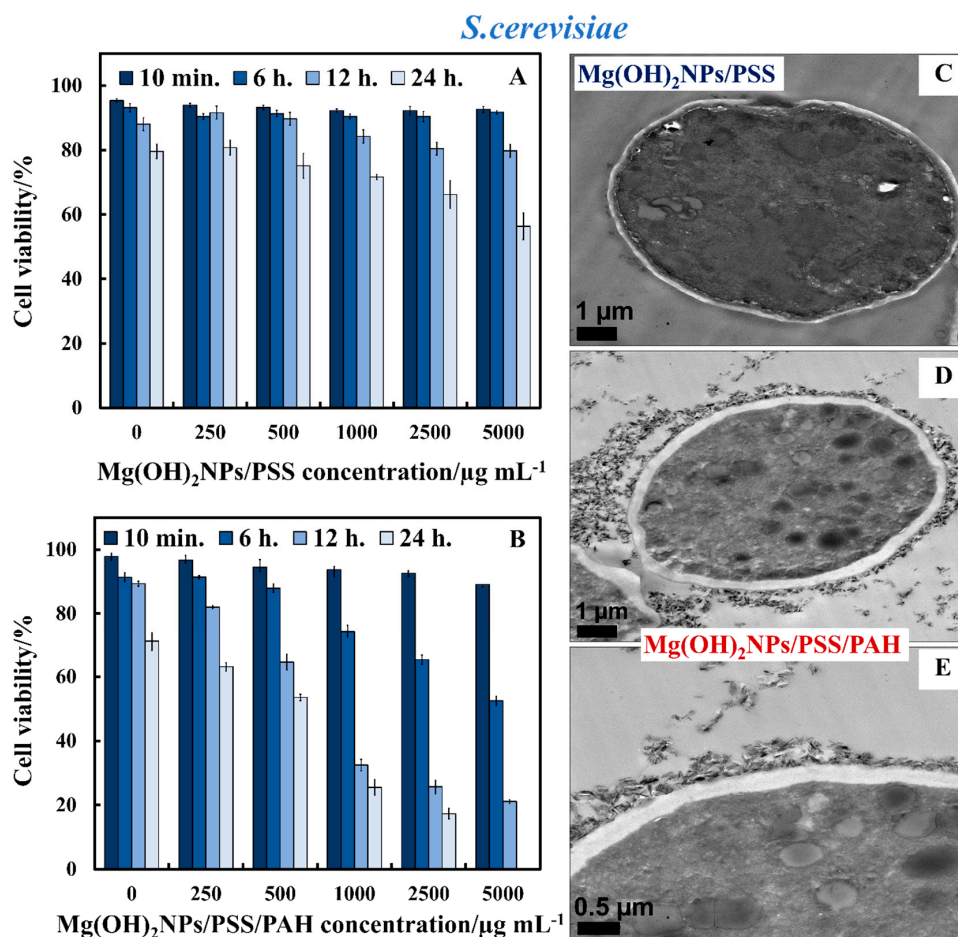
Figure 9. *S. cerevisiae* cell viability as a function of nanoparticle concentration after incubation for up to 24 h with (**A**) Mg(OH)$_2$NPs/PSS and (**B**) Mg(OH)$_2$NPs/PSS/PAH. TEM images of *S. cerevisiae* cells incubated for 24 h with (**C**) Mg(OH)$_2$NPs/PSS and (**D,E**) Mg(OH)$_2$NPs/PSS/PAH at different magnifications.

Hence, by coating the Mg(OH)$_2$NPs with an outer layer of anionic polyelectrolyte, their antimicrobial activity is significantly decreased because of the electrostatic repulsion between the anionic Mg(OH)$_2$NPs/PSS and the anionic surface of *S. cerevisiae* cells. Figure 9C–E show TEM images of *S. cerevisiae* cells after their incubation with Mg(OH)$_2$NPs that were coated with PSS and PAH layers.

The TEM image in Figure 9C indirectly confirms the lack of nanoparticle accumulation due to the electrostatic repulsion among the anionic Mg(OH)$_2$NPs/PSS and the negatively charged *S. cerevisiae* cell wall. Figure 9D,E show the great accumulation of Mg(OH)$_2$NPs/PSS/PAH on the cell walls, which corresponds to a much higher activity towards *S. cerevisiae*. One can conclude that coating Mg(OH)$_2$NPs with PSS as an external layer significantly diminishes their ability to attach on the treated cells, as shown in Figure 9C. *S. cerevisiae* cell viability tests revealed that Mg(OH)$_2$NPs/PSS were much less effective in killing the cells than the Mg(OH)$_2$NPs/PSS/PAH or bare Mg(OH)$_2$NPs, which strongly accumulate on the cell membrane due to electrostatic attraction. These results were

also supported by the TEM images of *S. cerevisiae*. Figure S16 shows the same data as Figure 9A,B in CFU ml^{-1}. Figure 10A,B compares the antimicrobial activity of multilayer-coated Mg(OH)$_2$NPs with PSS and PAH polyelectrolytes at various NPs concentrations on the *C. reinhardtii*. Figure 10A shows that, for incubating times of up to 6 h, no measurable variation in the *C. reinhardtii* cell viability was detected for Mg(OH)$_2$NPs/PSS, even at high particle concentrations. However, at similar conditions, the cationic Mg(OH)$_2$NPs/PSS/PAH displayed a marked antimicrobial activity on *C. reinhardtii*, even at 250 μg mL^{-1}. A very strong effect of the Mg(OH)$_2$NPs/PSS/PAH on the *C. reinhardtii* cells viability was observed for exposure times of up to six hours at 1000 μg mL^{-1} particle concentrations (Figure 10B). One can conclude that, by coating the Mg(OH)$_2$NPs with an external layer of anionic polyelectrolyte, their antimicrobial activity decreased for both *S. cerevisiae* and *C. reinhardtii,* because of the electrostatic repulsion between the Mg(OH)$_2$NPs/PSS and the cells walls. Figure 10C–E confirm this hypothesis with TEM images of *C. reinhardtii* exposed into the polyelectrolyte-coated Mg(OH)$_2$NPs. We also conducted similar tests with Gram-negative bacteria (*E. coli*) and polyelectrolyte-coated Mg(OH)$_2$NPs when the bacterial cells were removed from their culture media. Figure S17 (ESI) shows the same data as Figure 10A,B in CFU mL^{-1}. Figure S13 compares the anti-yeast activity bare Mg(OH)$_2$NPs with Mg(OH)$_2$NPs/PSS and Mg(OH)$_2$NPs/PSS/PAH as a function of the nanoparticle concentration for 24 h of exposure.
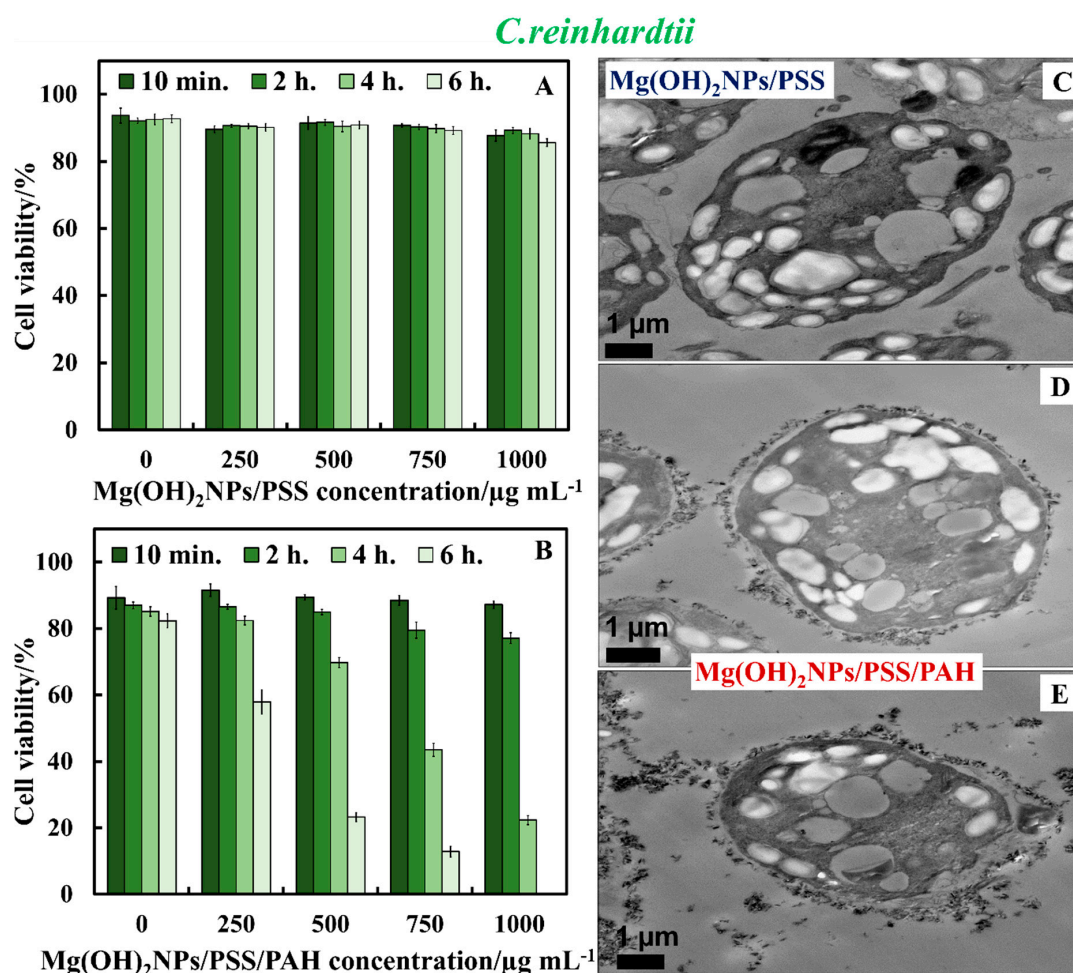
Figure 10. *C. reinhardtii* cell viability as a function of nanoparticle concentration after incubation for up to 6 h with (**A**) Mg(OH)$_2$NPs/PSS and (**B**) Mg(OH)$_2$NPs/PSS/PAH. TEM images of *C. reinhardtii* after being incubated for 6 h with (**C**) 1000 μg mL^{-1} Mg(OH)$_2$NPs/PSS, (**D**) 750 μg mL^{-1} Mg(OH)$_2$NPs /PSS/PAH, and (**E**) 1000 μg mL^{-1} of Mg(OH)$_2$NPs /PSS/PAH.

Figure 11A,B show the effect of polyelectrolyte multilayer-coated $Mg(OH)_2NPs$ against *E. coli*. Similarly to *S. cerevisiae* and *C. reinhardtii,* we found no pronounced antibacterial effect of $Mg(OH)_2NPs/PSS$ on *E. coli* for various exposure times. Figure 11A shows that the antibacterial activity of $Mg(OH)_2NPs/PSS$ against *E. coli* is also much lower than the one of the bare $Mg(OH)_2NPs$. We envisage that this result is due to a similar decrease of the NPs accumulation on the bacterial cell wall after the functionalization of the $Mg(OH)_2NPs$ with an anionic PSS layer (see Figure 11C,D,F,G). The subsequent deposition of a cationic polyelectrolyte layer of PAH, yields $Mg(OH)_2NPs/PSS/PAH$, which showed excellent antibacterial properties against *E. coli*, as seen in Figure 11B. Note that the PAH-coated NPs have even stronger antibacterial activity than the uncoated $Mg(OH)_2NPs$ towards *E. coli*. Hence, the antibacterial activity of the polyelectrolyte coated $Mg(OH)_2NPs$ appears to alternate with their surface charge. Figure S18 (ESI) shows the same data as in Figure 10A,B in CFU mL^{-1}.
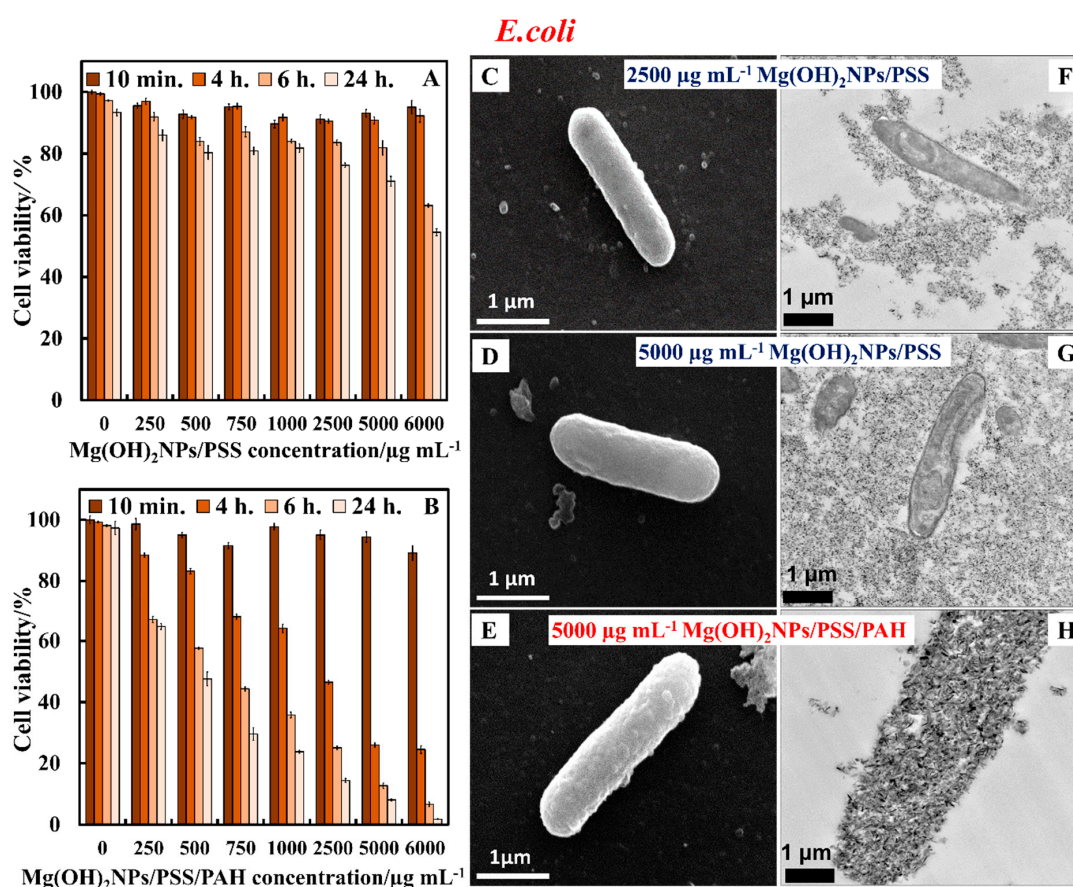
Figure 11. The *E. coli* cell viability after treatment with (**A**) $Mg(OH)_2NPs/PSS$ and (**B**) $Mg(OH)_2NPs/PSS/PAH$ for various incubation times as a function of the NPs concentration. (**C**) SEM and (**F**) TEM images of *E. coli* after incubation with 2500 μg mL^{-1} $Mg(OH)_2NPs/PSS$; (**D**) SEM and (**G**) TEM images of *E. coli* after incubation with 5000 μg mL^{-1} $Mg(OH)_2NPs/PSS$; (**E**) SEM and (**H**) TEM images of *E. coli* after incubation with 5000 μg mL^{-1} $Mg(OH)_2NPs/PSS/PAH$. The cells were removed from the particle suspension before the sample preparation for TEM and SEM imaging.

The *E. coli* Gram-negative cell wall is composed of an organized triple membrane that contains a thin inner layer of peptidoglycan between an outer membrane consisting of porins [41], phospholipids molecules, lipopolysaccharides (LPS), lipoproteins, surface proteins, and a cytoplasmic membrane consisting of phospholipids molecules and porins (see Figure S10) [41]. Figure 11C–H show the SEM and TEM images of *E. coli* after treatment for 24 h with $Mg(OH)_2NPs$ coated with a single layer of PSS and ones with additional layer of PAH. Note that there are a very few $Mg(OH)_2NPs/PSS$ that are attached to the bacteria, as shown in Figure 11C,D,F,G. On the other hand, we found a significant accumulation

of Mg(OH)$_2$NPs/PSS/PAH onto the surface of the bacteria, as shown in Figure 11E,H. These SEM and TEM images are consistent with the antibacterial activity profile of the polyelectrolyte-coated Mg(OH)$_2$NPs against *E. coli,* as reported in Figure 11B. It can be argued that the weak attachment of the anionic particles Mg(OH)$_2$NPs/PSS to the bacteria, as supported via the SEM and TEM images, causes little damage of the bacteria wall. Figure 7B,C,E,F for the bare Mg(OH)$_2$NPs and Figure 11E,H for the Mg(OH)$_2$NPs/PSS/PAH, show that there is a substantial build-up of cationic NPs (uncoated and PAH-coated Mg(OH)$_2$NPs) onto the anionic bacterial cell surface, which corresponds to a greater local increase of the NPs concentration that successively disrupts the bacteria. Figure S14 compares the anti-yeast activity bare Mg(OH)$_2$NPs with Mg(OH)$_2$NPs/PSS and Mg(OH)$_2$NPs/PSS/PAH as a function of the nanoparticle concentration for 24 h of exposure. We also examined the antibacterial activity of MgCl$_2$ solutions of various concentrations for 24 h on *E. coli* in order to investigate if this is due to higher local concentration of Mg^{2+} ions, where the bacterial cells were extracted from the culture media in a similar processes, as explained above for the Mg(OH)$_2$NPs treatment with *E. coli*. We found that MgCl$_2$ did not have significant antibacterial action when compared to the Mg(OH)$_2$NPs, even at high concentrations, as shown in Figure S11 (ESI). The effect of the pH on the bacterial cell viability is similar—we found that the incubation of bacteria with NaOH solution of pH 10.4 (corresponding to the pH of bare Mg(OH)$_2$NPs suspension) did not produce a comparable effect. Hence, the analysis of these results suggests that magnesium ions in the Mg(OH)$_2$NPs and the basic pH of 10.4 is unlikely to be responsible for the killing of *E. coli* [28]. The most likely explanation is the rough surface morphology of the clustered Mg(OH)$_2$NPs, which, when electrostatically attracted towards the cell membrane, cause membrane disruptions that kill the bacteria.

Note that neither Mg^{2+} ions nor reactive oxygen species (ROS) generation can explain the antimicrobial properties of the Mg(OH)$_2$NPs. The solubility of Mg(OH)$_2$NPs is too low for the free Mg^{2+} ions to have any measurable cytotoxic effect, as their concentration is limited by the solubility product of Mg(OH)$_2$NPs (1.8×10^{-11} M^3). The Mg(OH)$_2$NPs are not a photoactive material, which means that it is not producing ROS upon illumination. Hence, the antimicrobial effect is likely coming from the surface roughness of the Mg(OH)$_2$NPs, which electrostatically stick onto the negatively charged microbial cells due to their cationic character and pierce their cell membrane. The effect is also amplified by the high concentration of OH- ions in their electric double layers, which they bring in close contact with the microbial cell surface upon adhesion. This can potentially lead to partial hydrolysis of the lipids in their cell membranes and cell death.

We also determined the MIC of free Mg(OH)$_2$NPs and PAH-coated Mg(OH)$_2$NPs on *E. coli*, *S. cerevisiae,* and *C. reinhardtii.* We found that, at the same conditions, the MIC of the PAH-coated Mg(OH)$_2$NPs is two times lower than that of free Mg(OH)$_2$NPs (see Table 1).

Table 1. Minimum inhibitory concentration (MIC) of bare Mg(OH)$_2$NPs and PSS/PAH-coated Mg(OH)$_2$NPs against *C. reinhardtii, S. cerevisiae* and *E. coli*.

	Mg(OH)$_2$NPs	PSS/PAH-coated Mg(OH)$_2$NPs
	MIC	MIC
C. reinhardtii	1000 μg mL^{-1}	750 μg mL^{-1}
S. cerevisiae	5000 μg mL^{-1}	2500 μg mL^{-1}
E. coli	5000 μg mL^{-1}	2500 μg mL^{-1}

3.7. Effect of the bare Mg(OH)$_2$NPs and PSS/PAH-coated Mg(OH)$_2$NPs on human cells

Figure S19 (ESI) shows the cytotoxicity assay of the bare Mg(OH)$_2$NPs and Mg(OH)$_2$NPs/PSS/PAH on human embryonic kidney cells (HEK 293 cell line) for up to 24 h of exposure. The cells were removed from the original culture media and then transferred to PBS before exposure to the nanoparticles. This was done to avoid the adsorption of the media components on the particles. Both runs were done at the varying overall nanoparticles concentration and at different incubation times. One can see a very

small effect on the presence of free Mg(OH)$_2$NPs and Mg(OH)$_2$NPs/PSS/PAH on the cells viability over a period of up to 24 h. Note that the control sample of HEK 293 cells has lost a minor fraction of their viability over this period of time due to the removal of the culture media. One can conclude that the nanoparticle does not measurably impact the HEK 292 cell viability up to 2500 µg mL^{-1}. However, the effect on yeast, algae, and *E. coli* is very significant at these concentrations of free Mg(OH)$_2$NPs and Mg(OH)$_2$NPs/PSS/PAH—see Figures 4, 9B, 10B and 11B, respectively. Therefore, one may conclude that the Mg(OH)$_2$NPs show excellent biocompatibility with this human cell line. More research will be conducted in the future regarding the effects of the nanoparticles on different type of other cell lines.

4. Conclusions

When compared with other inorganic nanoparticles that were studied in the literature, Mg(OH)$_2$NPs have high antimicrobial activity at moderate to high particle concentrations. However, the Mg(OH)$_2$NPs have great application potential as a new antimicrobial agent, since Mg(OH)$_2$ is a nontoxic material and has been broadly used in medical industries and food. Here, we studied various ways to control the antimicrobial activity and cytotoxicity of a range of bare and surface-modified Mg(OH)$_2$NPs on three different types of microbial cells: microalgae, yeast, and bacteria. The antimicrobial activity of the Mg(OH)$_2$NPs on *S. cerevisiae*, *C. reinhardtii*, and *E. coli* was examined. This work suggests that bare Mg(OH)$_2$NPs are effective antimicrobial agents. The results from TEM and SEM analysis showed that the direct contact between the Mg(OH)$_2$NPs and the cell membrane of *S. cerevisiae*, *C. reinhardtii*, and *E. coli* is very important for their effective antimicrobial action. A series of polyelectrolyte-coated Mg(OH)$_2$NPs were likewise synthesised while using the layer by-layer technique and their antimicrobial activity towards *S. cerevisiae*, *C. reinhardtii*, and *E. coli* was compared with that of bare Mg(OH)$_2$NPs in order to evaluate the role of the surface coating. It was discovered that the antimicrobial activity of the coated Mg(OH)$_2$NPs alternates with their surface charge. The anionic nanoparticles (Mg(OH)$_2$NPs/PSS) have much lower antibacterial activity than the cationic ones (Mg(OH)$_2$NPs/PSS/PAH and bare Mg(OH)$_2$NPs). We also show that Mg(OH)$_2$NPs/PSS/PAH and bare Mg(OH)$_2$NPs have only very minor impact on selected human cells line (HEK293), which implies good biocompatibility. This can bring important insights as to how the antmicrobial properties of Mg(OH)$_2$NPs and other inorganic nanoparticles can be controlled by designing nanoparticle surface coatings that promote their adhesion to the microbial cell walls, as well as by taking into account the nanoparticles surface morphology.

concentrations on *E. coli.*, Figure S21. The anti-yeast, anti-algal and antibacterial activity of free PAH at various concentrations on (A) *S. cerevisiae*, (B) *C. reinhardtii* (C) *E. coli.*

References

1.　Lee, D.; Cohen, R.E.; Rubner, M.F. Antibacterial properties of Ag nanoparticle loaded multilayers and formation of magnetically directed antibacterial microparticles. *Langmuir* **2005**, *21*, 9651–9659. [CrossRef] [PubMed]

2.　Rawlinson, L.A.B.; Ryan, S.M.; Mantovani, G.; Syrett, J.A.; Haddleton, D.M.; Brayden, D.J. Antibacterial effects of poly (2-(dimethylamino ethyl) methacrylate) against selected gram-positive and gram-negative bacteria. *Biomacromolecules* **2009**, *11*, 443–453. [CrossRef] [PubMed]

3.　Muñoz-Bonilla, A.; Fernández-García, M. Polymeric materials with antimicrobial activity. *Prog. Polym. Sci.* **2012**, *37*, 281–339. [CrossRef]

4.　Halbus, A.F.; Horozov, T.S.; Paunov, V.N. Strongly enhanced antibacterial action of copper oxide nanoparticles with boronic acid surface functionality. *ACS Appl. Mater. Inter.* **2019**, *11*, 12232–12243. [CrossRef] [PubMed]

5.　Halbus, A.F.; Horozov, T.S.; Paunov, V.N. Self-grafting copper oxide nanoparticles show a strong enhancement of their anti-algal and anti-yeast action. *Nanoscale Adv.* **2019**, *1*, 2323–2336. [CrossRef]

6.　Vatsha, B.; Tetyana, P.; Shumbula, P.M.; Ngila, J.C.; Sikhwivhilu, L.M.; Moutloali, R.M. Effects of precipitation temperature on nanoparticle surface area and antibacterial behaviour of $Mg(OH)_2$ and MgO nanoparticles. *J. Biomater. Nanobiotechnol.* **2013**, *4*, 365–373. [CrossRef]

7.　Al-Obaidy, S.S.; Halbus, A.F.; Greenway, G.M.; Paunov, V.N. Boosting the antimicrobial action of vancomycin formulated in shellac nanoparticles of dual-surface functionality. *J. Mater. Chem. B.* **2019**, *7*, 3119–3133. [CrossRef]

8.　Weldrick, P.J.; Iveson, S.; Hardman, M.J.; Paunov, V.N. Breathing new life into old antibiotics: Overcoming antibacterial resistance by antibiotic-loaded nanogel carriers with cationic surface functionality. *Nanoscale* **2019**, *11*, 10472–10485. [CrossRef]

9.　Halbus, A.F.; Horozov, T.S.; Paunov, V.N. Colloid particle formulations for antimicrobial applications. *Adv. Colloid Interface Sci.* **2017**, *249*, 134–148. [CrossRef]

10.　Zhang, H.; Chen, B.; Banfield, J.F. Particle Size and pH Effects on Nanoparticle Dissolution. *J. Phys. Chem. C* **2010**, *114*, 14876–14884. [CrossRef]

11.　Liu, J.; Aruguete, D.M.; Murayama, M.; Hochella, M.F., Jr. Influence of size and aggregation on the reactivity of an environmentally and industrially relevant nanomaterial (PbS). *Environ. Sci. Technol.* **2009**, *43*, 8178–8183. [CrossRef] [PubMed]

12.　Zhang, Y.; Chen, Y.; Westerhoff, P.; Hristovski, K.; Crittenden, J.C. Stability of commercial metal oxide nanoparticles in water. *Water Res.* **2008**, *42*, 2204–2212. [CrossRef] [PubMed]

13.　Petosa, A.R.; Jaisi, D.P.; Quevedo, I.R.; Elimelech, M.; Tufenkji, N. Aggregation and deposition of engineered nanomaterials in aquatic environments: Role of physicochemical interactions. *Environ. Sci. Technol.* **2010**, *44*, 6532–6549. [CrossRef] [PubMed]

14.　Sada, E.; Kumazawa, H.; Sawada, Y.; Kondo, T. Simultaneous absorption of dilute nitric oxide and sulfur dioxide into aqueous slurries of magnesium hydroxide with added iron (II)-EDTA chelate. *Ind. Eng. Chem. Process Des. Dev.* **1982**, *21*, 771–774. [CrossRef]

15.　Gui, H.; Zhang, X.; Dong, W.; Wang, Q.; Gao, J.; Song, Z.; Lai, J.; Liu, Y.; Huang, F.; Qiao, J. Flame retardant synergism of rubber and $Mg(OH)_2$ in EVA composites. *Polymer* **2007**, *48*, 2537–2541. [CrossRef]

16. Cao, H.; Zheng, H.; Yin, J.; Lu, Y.; Wu, S.; Wu, X.; Li, B. $Mg(OH)_2$ complex nanostructures with superhydrophobicity and flame-retardant effects. *J. Phys. Chem. C* **2010**, *114*, 17362–17368. [CrossRef]

17. Pan, X.; Wang, Y.; Chen, Z.; Pan, D.; Cheng, Y.; Liu, Z.; Lin, Z.; Guan, X. Investigation of antibacterial activity and related mechanism of a series of nano-$Mg(OH)_2$. *ACS Appl. Mater. Interfaces* **2013**, *5*, 1137–1142. [CrossRef]

18. Martin, P.D.; Schneck, D.W.; Dane, A.L.; Warwick, M.J. The effect of a combination antacid preparation containing aluminium hydroxide and magnesium hydroxide on rosuvastatin pharmacokinetics. *Curr. Med. Res. Opin.* **2008**, *24*, 1231–1235. [CrossRef]

19. Scott, G.; Reynolds, C.V.; Milosavljev, S.; Langholff, W.; Shenouda, M.; Rordorf, C. Lack of effect of omeprazole or of an aluminium hydroxide/magnesium hydroxide antacid on the pharmacokinetics of lumiracoxib. *Clin. Pharmacokinet.* **2004**, *43*, 341–348. [CrossRef]

20. Kang, J.; Schwendeman, S.P. Comparison of the effects of Mg $(OH)_2$ and sucrose on the stability of bovine serum albumin encapsulated in injectable poly (D,L-lactide-co-glycolide) implants. *Biomaterials* **2002**, *23*, 239–245. [CrossRef]

21. Tong, K.; Song, X.; Xiao, G.; Yu, J. Colloidal processing of Mg $(OH)_2$ aqueous suspensions using sodium polyacrylate as dispersant. *Ind. Eng. Chem. Res.* **2014**, *53*, 4755–4762. [CrossRef]

22. Waaijers, S.L.; Kong, D.; Hendriks, H.S.; de Wit, C.A.; Cousins, I.T.; Westerink, R.H.; Leonards, P.E.; Kraak, M.H.; Admiraal, W.; de Voogt, P. Persistence, bioaccumulation, and toxicity of halogen-free flame retardants. In *Reviews of Environmental Contamination and Toxicology*; Springer: New York, NY, USA, 2013; pp. 1–71.

23. Dong, C.; Song, D.; Cairney, J.; Maddan, O.L.; He, G.; Deng, Y. Antibacterial study of $Mg(OH)_2$ nanoplatelets. *Mater. Res. Bull.* **2011**, *46*, 576–582. [CrossRef]

24. Dong, C.; Cairney, J.; Sun, Q.; Maddan, O.L.; He, G.; Deng, Y. Investigation of Mg $(OH)_2$ nanoparticles as an antibacterial agent. *J. Nanopart. Res.* **2010**, *12*, 2101–2109. [CrossRef]

25. Dong, C.; He, G.; Li, H.; Zhao, R.; Han, Y.; Deng, Y. Antifouling enhancement of poly (vinylidene fluoride) microfiltration membrane by adding $Mg(OH)_2$ nanoparticles. *J. Membr. Sci.* **2012**, *387*, 40–47. [CrossRef]

26. Wang, Z.; Li, C.; Mu, Y.; Lin, Z.; Yi, A.; Zhang, Q.; Yan, B. Nanoadduct relieves: Alleviation of developmental toxicity of Cr(VI) due to its spontaneous adsorption to $Mg(OH)_2$ nanoflakes. *J. Hazard. Mater.* **2015**, *287*, 296–305. [CrossRef] [PubMed]

27. Pilarska, A.; Bula, K.; Myszka, K.; Rozmanowski, T.; Szwarc-Rzepka, K.; Pilarski, K.; Chrzanowski, Ł.; Czaczyk, K.; Jesionowski, T. Functional polypropylene composites filled with ultra-fine magnesium hydroxide. *Open Chem.* **2015**, *13*, 161–171. [CrossRef]

28. Dong, C.; He, G.; Zheng, W.; Bian, T.; Li, M.; Zhang, D. Study on antibacterial mechanism of $Mg(OH)_2$ nanoparticles. *Mater. Lett.* **2014**, *134*, 286–289. [CrossRef]

29. Li, Q.; Mahendra, S.; Lyon, D.Y.; Brunet, L.; Liga, M.V.; Li, D.; Alvarez, P.J. Antimicrobial nanomaterials for water disinfection and microbial control: Potential applications and implications. *Water Res.* **2008**, *42*, 4591–4602. [CrossRef]

30. Mendonca, A.F.; Amoroso, T.L.; Knabel, S.J. Destruction of gram-negative food-borne pathogens by high pH involves disruption of the cytoplasmic membrane. *Appl. Environ. Microbiol.* **1994**, *60*, 4009–4014.

31. Kumar, A.; Vemula, P.K.; Ajayan, P.M.; John, G. Silver-nanoparticle-embedded antimicrobial paints based on vegetable oil. *Nat. Mater.* **2008**, *7*, 236–241. [CrossRef]

32. Hoshino, A.; Fujioka, K.; Oku, T.; Suga, M.; Sasaki, Y.F.; Ohta, T.; Yasuhara, M.; Suzuki, K.; Yamamoto, K. Physicochemical properties and cellular toxicity of nanocrystal quantum dots depend on their surface modification. *Nano Lett.* **2004**, *4*, 2163–2169. [CrossRef]

33. Mudunkotuwa, I.A.; Grassian, V.H. Citric acid adsorption on TiO_2 nanoparticles in aqueous suspensions at acidic and circumneutral pH: Surface coverage, surface speciation, and its impact on nanoparticle–nanoparticle interactions. *J. Am. Chem. Soc.* **2010**, *132*, 14986–14994. [CrossRef] [PubMed]

34. LB (Luria-Bertani) liquid medium. *Cold Spring Harb. Protoc.* **2006**. [CrossRef]

35. Al-Awady, M.J.; Greenway, G.M.; Paunov, V.N. Nanotoxicity of polyelectrolyte-functionalized titania nanoparticles towards microalgae and yeast: Role of the particle concentration, size and surface charge. *RSC Adv.* **2015**, *5*, 37044–37059. [CrossRef]

36. Yu, J.C.; Xu, A.; Zhang, L.; Song, R.; Wu, L. Synthesis and characterization of porous magnesium hydroxide and oxide nanoplates. *J. Phys. Chem. B* **2004**, *108*, 64–70. [CrossRef]

37. Dhaouadi, H.; Chaabane, H.; Touati, F. Mg(OH)$_2$ nanorods synthesized by a facile hydrothermal method in the presence of CTAB. *Nano Micro Lett.* **2011**, *3*, 153–159. [CrossRef]

38. Meshkani, F.; Rezaei, M. Facile synthesis of nanocrystalline magnesium oxide with high surface area. *Powder Technol.* **2009**, *196*, 85–88. [CrossRef]

39. Pang, H.; Ning, G.; Gong, W.; Ye, J.; Lin, Y. Direct synthesis of hexagonal Mg(OH)$_2$ nanoplates from natural brucite without dissolution procedure. *Chem. Commun.* **2011**, *47*, 6317–6319. [CrossRef]

40. Wu, X.F.; Hu, G.S.; Wang, B.B.; Yang, Y.F. Synthesis and characterization of superfine magnesium hydroxide with monodispersity. *J. Cryst. Growth* **2008**, *310*, 457–461. [CrossRef]

41. Brayner, R.; Ferrari-Iliou, R.; Brivois, N.; Djediat, S.; Benedetti, M.F.; Fiévet, F. Toxicological impact studies based on *Escherichia coli* bacteria in ultrafine ZnO nanoparticles colloidal medium. *Nano Lett.* **2006**, *6*, 866–870. [CrossRef]

42. Lin, W.; Xu, Y.; Huang, C.C.; Ma, Y.; Shannon, K.B.; Chen, D.R.; Huang, Y.W. Toxicity of nano-and micro-sized ZnO particles in human lung epithelial cells. *J. Nanopart. Res.* **2009**, *11*, 25–39. [CrossRef]

43. Sondi, I.; Salopek-Sondi, B. Silver nanoparticles as antimicrobial agent: A case study on *E. coli* as a model for Gram-negative bacteria. *J. Colloid Interface Sci.* **2004**, *275*, 177–182. [CrossRef] [PubMed]

44. Al-Awady, M.J.; Fauchet, A.; Greenway, G.M.; Paunov, V.N. Enhanced antimicrobial effect of berberine in nanogel carriers with cationic surface functionality. *J. Mater. Chem. B* **2017**, *5*, 7885–7897. [CrossRef]

45. Al-Awady, M.J.; Weldrick, P.J.; Hardman, M.J.; Greenway, G.M.; Paunov, V.N. Amplified antimicrobial action of chlorhexidine encapsulated in PDAC-functionalized acrylate copolymer nanogel carriers. *Mater. Chem. Front.* **2018**, *2*, 2032–2044. [CrossRef]

46. Franklin, N.M.; Rogers, N.J.; Apte, S.C.; Batley, G.E.; Gadd, G.E.; Casey, P.S. Comparative toxicity of nanoparticulate ZnO, bulk ZnO, and ZnCl$_2$ to a freshwater microalga (*Pseudokirchneriella subcapitata*): The importance of particle solubility. *Environ. Sci. Technol.* **2007**, *41*, 8484–8490. [CrossRef] [PubMed]

47. Heinlaan, M.; Ivask, A.; Blinova, I.; Dubourguier, H.C.; Kahru, A. Toxicity of nanosized and bulk ZnO, CuO and TiO$_2$ to bacteria *Vibrio fischeri* and crustaceans *Daphnia magna* and *Thamnocephalus platyurus*. *Chemosphere* **2008**, *71*, 1308–1316. [CrossRef] [PubMed]

48. Choi, O.; Hu, Z. Size dependent and reactive oxygen species related nanosilver toxicity to nitrifying bacteria. *Environ. Sci. Technol.* **2008**, *42*, 4583–4588. [CrossRef] [PubMed]

49. Pan, Y.; Neuss, S.; Leifert, A.; Fischler, M.; Wen, F.; Simon, U.; Schmid, G.; Brandau, W.; Jahnen-Dechent, W. Size-dependent cytotoxicity of gold nanoparticles. *Small* **2007**, *3*, 1941–1949. [CrossRef]

50. Al-Obaidy, S.S.; Greenway, G.M.; Paunov, V.N. Dual-functionalised shellac nanocarriers give a super-boost of the antimicrobial action of berberine. *Nanoscale Adv.* **2019**, *1*, 858–872. [CrossRef]

51. Chen, P.; Powell, B.A.; Mortimer, M.; Ke, P.C. Adaptive interactions between zinc oxide nanoparticles and *Chlorella* sp. *Environ. Sci. Technol.* **2012**, *46*, 12178–12185. [CrossRef]